Virologica Sinica 41 (2026) 413–422

Contents lists available at ScienceDirect

Virologica Sinica

journal homepage: www.keaipublishing.com/en/journals/virologica-sinica
www.virosin.org

Research Article

Nanobody targeting glycan cap confers broad orthoebolavirus neutralization

Xinhui Zhang [a,b], Yi Liao [a,b], Xiuying Liu [a,b], Jingya Zhou [a,b], Peixiang Gao [a,b], Xuemeng Dong [a,b], Shengnan Pan [a,b], Huarui Duan [a,b], Junyu Liu [a,b], Xiaojing Chi [a,b,*], Wei Yang [a,b,c,*]

[a] Key Laboratory of Pathogen Infection Prevention and Control (Ministry of Education), National Institute of Pathogen Biology, Chinese Academy of Medical Sciences & Peking Union Medical College, Beijing 102629, China
[b] NHC Key Laboratory of Systems Biology of Pathogens, National Institute of Pathogen Biology, Chinese Academy of Medical Sciences & Peking Union Medical College, Beijing 102629, China
[c] State Key Laboratory of Respiratory Health and Multimorbidity, Chinese Academy of Medical Sciences & Peking Union Medical College, Beijing 100730, China

ARTICLE INFO

Keywords:
Nanobody
Orthoebolavirus
Neutralizing antibody
Glycan cap
Broad-spectrum

ABSTRACT

The Zaire Ebola virus (EBOV) and Bundibugyo virus (BDBV) cause severe hemorrhagic fever with high mortality, highlighting the urgent need for broad-spectrum antiviral therapies. Neutralizing nanobodies, with their small size, structural stability, and ability to access sterically restricted epitopes, represent a promising antiviral modality. Here, we identified a high-affinity nanobody, BDBV-Nb02, from a fully synthetic phage display library targeting the glycan cap of BDBV glycoprotein (GP1). BDBV-Nb02 demonstrated strong binding kinetics (KD ≈ 1 nM) and potent neutralizing activity against both BDBV and EBOV pseudoviruses, with half-maximal inhibitory concentration (IC_{50}) values in the nanomolar range. Engineering a bivalent format significantly enhanced neutralization potency, achieving up to a 56-fold reduction in the 90% inhibitory concentration (IC_{90}) compared with the monovalent form. Epitope competition assays and molecular docking revealed that BDBV-Nb02 targets a conserved glycan cleft, with residues F248 and NP278/279 identified as critical neutralization sites. In contrast, Fc-fusion constructs impaired the nanobody's efficacy, highlighting the importance of preserving the structural features that enable access to glycan-shielded epitopes. Our findings demonstrate that BDBV-Nb02 is a promising candidate for broad-spectrum orthoebolavirus therapy and may serve as a valuable component in future antiviral cocktail formulations.

INTRODUCTION

Orthoebolaviruses (formerly Ebolaviruses) are members of the family *Filoviridae* and cause severe hemorrhagic fever with case fatality rates ranging from 25% to 90%. (Feldmann and Geisbert, 2011; Rivera and Messaoudi, 2016). Six species are identified within the *Orthoebolavirus* genus: *Orthoebolavirus zairense* (Ebola virus, EBOV), *Orthoebolavirus sudanense* (Sudan virus, SUDV), *Orthoebolavirus taiense* (Taï Forest virus, TAFV), *Orthoebolavirus bundibugyoense* (Bundibugyo virus, BDBV), *Orthoebolavirus restonense* (Reston virus, RESTV), and *Orthoebolavirus bombaliense* (Bombali virus, BOMV). Among these, EBOV, BDBV, and SUDV are highly pathogenic and pose major threats to global health (Hutchinson and Rollin, 2007; Wauquier et al., 2010; Escudero-Pérez et al., 2014; Schieffelin et al., 2014; Caballero et al., 2016; Younan et al., 2017, 2018). Since the devastating 2013–2016 West African outbreak, recurrent epidemics have highlighted the urgent need for effective antiviral countermeasures.

The pathogenesis of orthoebolavirus infection is largely mediated by its surface glycoprotein (GP; GP1 and GP2), the critical determinant of viral entry. GP is rich in N- and O-linked glycans, functioning both as a 'key' for host cell entry and as a 'disguise' to evade host immune responses (Lee et al., 2008). In addition to the membrane-anchored GP, orthoebolavirus produces substantial amounts of soluble GP (sGP), which consists predominantly of GP1 and a small portion of GP2 but

* Corresponding authors.
E-mail addresses: chixiaojing@ipbcams.ac.cn (X. Chi), wyang@ipb.pumc.edu.cn (W. Yang).
Peer review under the responsibility of editorial board of *Virologica Sinica*.

https://doi.org/10.1016/j.virs.2026.03.018
Received 15 September 2025; Accepted 31 March 2026
Available online 8 April 2026

lacks the transmembrane and fusion domains (Pallesen et al., 2016). Secreted as a dimer, sGP acts as an immune decoy, further diminishing the effectiveness of host antibody responses. Consequently, antibodies targeting GP1 epitopes are often compromised by extensive glycosylation and sGP-mediated competition, leading to reduced neutralizing efficacy. Moreover, at sub-neutralizing concentrations, Fc-mediated antibody-dependent enhancement (ADE) may occur, highlighting the need for alternative antibody formats that mitigate this risk. Although several antibody-based therapies have been approved or advanced to clinical use for Ebola virus disease, such as Inmazeb (REGN-EB3) and ansuvimab (mAb114), which have demonstrated clinical efficacy (Corti et al., 2016; Mulangu et al., 2019), and ZMapp, which showed benefit during the 2014 epidemic, their activity is largely restricted to EBOV and remains limited against other orthoebolavirus species. As an RNA virus, orthoebolavirus exhibits substantial genetic diversity and a high mutation rate, necessitating the development and stockpiling of regional and species-specific variants.

Unlike traditional antibodies, nanobodies consist of only one variable region (VHH) of a heavy-chain antibody, with a molecular weight of approximately 12–15 kDa, about one-tenth that of typical antibodies. Their elongated CDR3 loops enable access to cryptic or recessed epitopes, such as the grooves and clefts on antigens that are often inaccessible to conventional antibodies (Yu et al., 2024). These properties make nanobodies particularly well suited to overcoming the epitope shielding imposed by extensive GP glycosylation. In addition, nanobodies exhibit extremely low toxicity and immunogenicity in humans (Steeland et al., 2016), and their lack of Fc region reduces the risk of ADE (Thomas et al., 2022). The clinical approval of the first nanobody-based therapeutic in 2019 (Scully et al., 2019), together with the successful development of potent SARS-CoV-2 nanobody inhibitors during the COVID-19 pandemic (Chi et al., 2020, 2022; Han et al., 2023), underscores their considerable therapeutic potential.

In this study, we screened a fully synthetic phage display library and identified a nanobody, BDBV-Nb02, which targets the glycan cap region of BDBV GP. We characterized its binding kinetics and neutralization activity against EBOV and BDBV pseudoviruses, and demonstrated that a bivalent format markedly enhances its neutralizing potency. Using epitope competition assays, site-directed mutagenesis, and molecular docking analyses, we further defined key residues involved in neutralization and elucidated the structural basis underlying its cross-reactive activity. Together, our work provides both a promising therapeutic candidate and new insights into nanobody engineering for combating Ebolavirus infections.

RESULTS

Nanoantibody identification and neutralizing activity

To identify nanobodies targeting Ebolaviruses, we used BDBV-GP1 lacking the mucin-like domain (MLD) as the screening antigen. The MLD is situated at the apex of each GP monomer and shields the receptor binding site (RBS) from immune recognition. Removal of the MLD does not alter the overall GP conformation, thereby allowing reliable antigen presentation. A fully synthetic nanobody phage display library was screened through four rounds of biopanning followed by phage ELISA, yielding 15 unique clones capable of binding BDBV GP1 (Supplementary Fig. S1). Selected nanobodies were expressed in *E. coli* and purified by nickel affinity chromatography (Supplementary Fig. S1).

To evaluate neutralization activity, pseudovirus bearing the glycoproteins of EBOV, BDBV, or SUDV were produced and tested in a BSL-2 system (Millet et al., 2019). Among the screened clones, two candidates (BDBV-Nb01 and BDBV-Nb02) exhibited measurable inhibitory activity. Neither nanobody neutralized SUDV pseudovirus; however, both displayed neutralizing activity against EBOV and BDBV, although complete neutralization was not achieved. Notably, the BDBV-Nb02 exhibited a significantly lower half-maximal inhibitory concentration (IC_{50}) than BDBV-Nb01 and achieved a maximal neutralization level of approximately 90% (Fig. 1).

Binding affinity and thermal stability of nanobodies

The binding kinetics of BDBV-Nb01 and BDBV-Nb02 were measured by surface plasmon resonance (SPR). BDBV GP1 was immobilized on a CM5 sensor chip, and serial dilutions of nanobodies were injected. BDBV-Nb02 bound GP1 with an equilibrium dissociation constant (KD) of approximately 1 nM, which was significantly stronger than that of BDBV-Nb01 (KD ≈ 16 nM) (Fig. 2A, B, and G). These binding characteristics were consistent with the neutralization assay, as BDBV-Nb02 displayed higher binding responses and slower dissociation kinetics than BDBV-Nb01. Further analysis of secondary structure via far-UV Circular Dichroism (CD) spectroscopy (190–260 nm) revealed that both nanobodies exhibited typical β-sheet double negative peaks at 208 nm and 222 nm (Fig. 2C and D). According to Fig. 2E and F, the melting temperatures (Tm) of BDBV-Nb01 and BDBV-Nb02 were 63.59 °C and 56.9 °C, respectively, indicating moderate thermal stability. Together, these results indicate that BDBV-Nb02 combines high affinity with moderate stability, supporting its potential as a therapeutic candidate.

Construction of bivalent nanobodies and neutralization enhancement

To overcome the limited neutralization of monovalent nanobodies, we designed dimeric nanobodies and Fc-fusion constructs aimed to improve antigen affinity, neutralizing, and pharmacokinetics profiles (Fig. 3A). BDBV-Nb01 and BDBV-Nb02 were engineered into four bivalent formats using flexible $GGGGS_5$ linkers: 1-1-HIS, 1-2-HIS, 2-1-HIS, and 2-2-HIS (Here, "1" and "2" represent BDBV-Nb01 and BDBV-Nb02, respectively). Among these constructs, only 2-2-HIS (BDBV-Nb02 homodimer) achieved complete neutralization of EBOV and BDBV pseudoviruses. Compared with the monomeric form, 2-2-HIS demonstrated a modest reduction in IC_{50} but a striking 56-fold improvement in 90% inhibitory concentration (IC_{90}) values, indicating a substantial gain in neutralization efficacy (Fig. 3B–D).

We also tested Fc-fusion constructs to evaluate pharmacological enhancement. Direct fusion of BDBV-Nb01 to Fc (1-FC) improved its neutralization ability compared to the monomer, but still inferior to 2-2-HIS. However, BDBV-Nb02-Fc fusion (2-FC) lost nearly all activity. When a $GGGGS_3$ linker was inserted between BDBV-Nb02 and Fc, named 2-FC ($GGGGS_3$), neutralizing activity was partially restored, but the neutralizing capacity remained inferior to that of 2-2-HIS. Other Fc-based constructs, 2-1-FC and 2-2-FC ($GGGGS_3$), exhibit nearly identical neutralization capacity against BDBV, showing a significant improvement in neutralizing activity compared to 2-FC ($GGGGS_3$), but none surpassed the bivalent 2-2-HIS format (Fig. 3E). SPR data revealed that the directly fused Fc construct (2-FC) exhibited significantly weaker affinity for BDBV GP1 compared to the monomer. While a flexible linker ($GGGGS_3$) partially restored binding, efficacy remained sub-optimal (Fig. 3F–I). We also attempted to use C-terminus Fc fusion and nanocage assembly strategies (Divine et al., 2021), but both approaches abolished neutralizing activity.

These results indicate that BDBV-Nb02 engages the glycan cleft of GP1 and that fully utilizes the characteristics of a nanobody, such as its small size and ultra-long CDR3 loop.

Epitopes identification of BDBV-Nb02

To further investigate the binding epitopes of BDBV-Nb02, we expressed and purified a panel of GP1-targeting antibodies in the 293F expression system (Rijal and Donnellan, 2023), as shown in Fig. 4A. EBOV-437 (magenta) and EBOV-548 (light green) have been reported to act in combination with EBOV-520, whereas EBOV-442 (light pink)

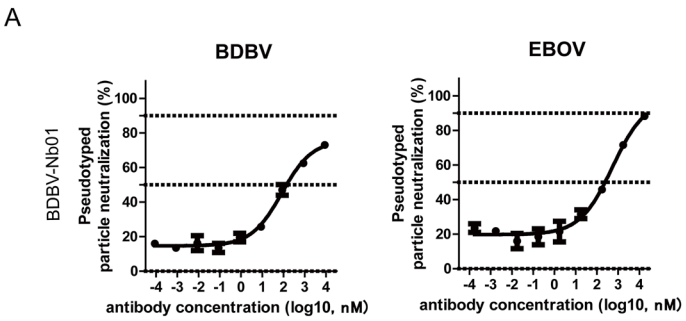

C

	BDBV		EBOV	
	IC_{50}	IC_{90}	IC_{50}	IC_{90}
BDBV-Nb01	579	/	240.5	/
BDBV-Nb02	2.4	683.9	9.4	319.9

Fig. 1. Pseudovirus neutralization activity of BDBV-Nb01 and BDBV-Nb02. Pseudoviruses were generated using an HIV-1 pNL4-3 backbone pseudotyped with the glycoproteins of Bundibugyo virus (BDBV) or Ebola virus (EBOV). Neutralization was assessed in Huh-7 cells using a 10-fold serial dilution series of each nanobody starting at 150 μg/mL. **A, B** Representative neutralization curves for BDBV-Nb01 (**A**) and BDBV-Nb02 (**B**). Percent inhibition was calculated relative to a no-antibody control. **C** Summary of half-maximal inhibitory concentration (IC_{50}) and 90% inhibitory concentration (IC_{90}) values for BDBV-Nb01 and BDBV-Nb02, shown as the mean of at least three independent experiments.

pairs with EBOV-515. The antibody 1C3 (orange) targets the receptor-binding domain (RBD) of GP protein and is commonly used in combination with 1C11.

Epitope competition was assessed by biofilm interference technology (BLI). BDBV GP1 antigen was immobilized on the AR2G biosensor via amino coupling. The four antibodies were used as primary antibodies to achieve saturated binding with BDBV-GP1, followed by saturated binding with each reference antibody. BDBV-Nb02 was added as the secondary antibody, and binding responses were monitored in real-time. Control experiments, in which the same antibody was applied as both primary and secondary, confirmed saturation and excluded non-specific effects (Fig. 4B).

Competition assays revealed that the RBD-targeting antibody 1C3 did not interfere with BDBV-Nb02, but BDBV-Nb02 strongly competed with EBOV-437 and EBOV-548, and there is partial epitope competition between BDBV-442 and BDBV-Nb02. These findings suggest that BDBV-Nb02 binds to a conserved glycan cap epitope distinct from the RBD. As BDBV-Nb02 strongly competed with BDBV-Nb01, consistent with neutralization results, bivalent nanobodies formed by BDBV-Nb01 and BDBV-Nb02 did not exhibit greater activity than 2-2-HIS.

We next compared the neutralizing activity of 2-2-HIS with EBOV-437 and EBOV-548 against EBOV and BDBV. While all three antibodies displayed comparable potency against EBOV, 2-2-HIS showed significantly stronger activity against BDBV, surpassing EBOV-437 and EBOV-548 (Fig. 4C). These results indicate that 2-2-HIS targets a conserved glycan cap epitope and exhibits robust cross-reactivity against EBOV and BDBV.

Identification of key neutralization sites

To investigate the molecular basis of BDBV-Nb02-mediated neutralization, we predicted the structure of BDBV-Nb02 using AlphaFold3 and performed docking analysis with BDBV GP (Fig. 5A). While AlphaFold3 reliably predicts individual structures, its accuracy for antibody-antigen interfaces remains limited, as illustrated by the inaccurate prediction of a known complex (ADI-15946-EBOV GP, PDB: 6MAM) (Supplementary Fig. S2). Therefore, rather than relying solely on computational predictions, we restricted the docking search space using our competition data (EBOV-437, EBOV-548, and BDBV-442), localizing the putative interface to GP1 residues Y220-D282. The resulting docking models (Fig. 5B) served purely as structural hypotheses for subsequent mutational validation.

Sequence alignment among EBOV, BDBV, and SUDV revealed five residues (L239, F248, K276, N278, P279) conserved between EBOV and BDBV but divergent in SUDV, consistent with the absence of SUDV neutralization (Fig. 5C and D). To exclude the possibility that the introduced point mutations might indirectly perturb global protein conformation, we generated pseudoviruses displaying BDBV GP harboring these SUDV-specific substitutions. Subsequent characterization confirmed that the mutant GP proteins retained wild-type levels of pseudovirus packaging efficiency and entry competence into Huh-7 cells

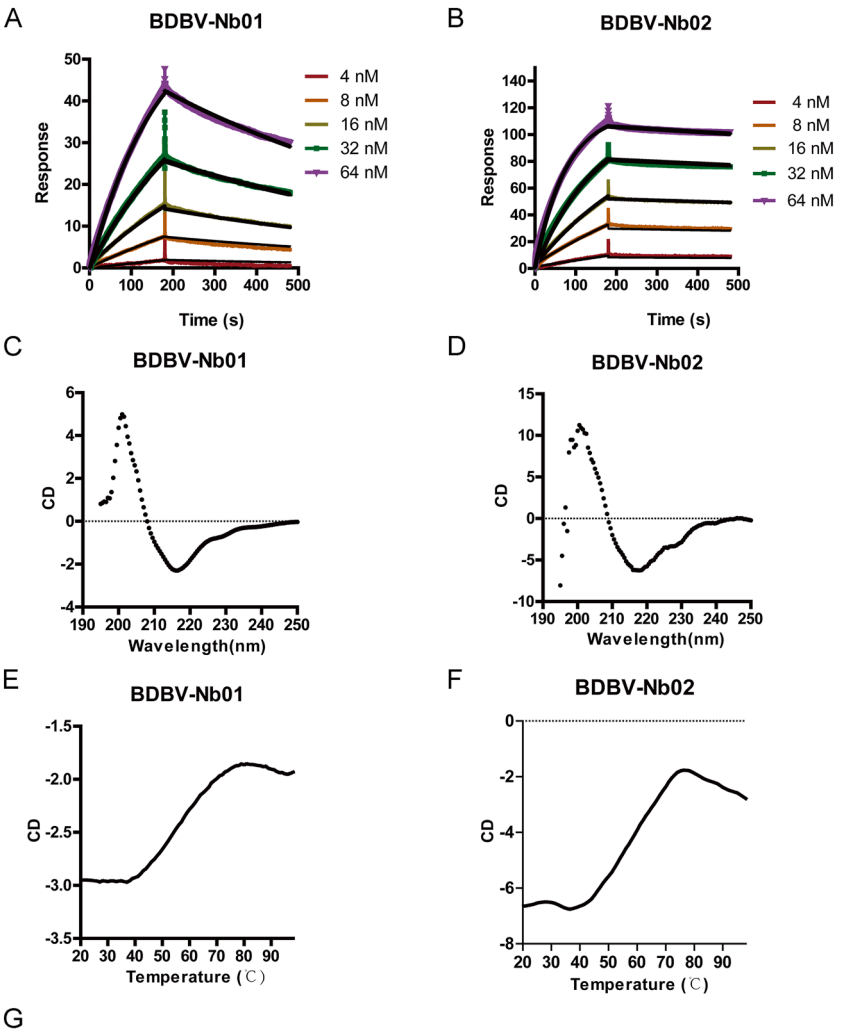

G

	K_D (nM)	K_{on} (M^{-1} S^{-1})	K_{off} (S^{-1})	Tm (℃)
BDBV-Nb01	16	7.94E+04	0.001274	63.59
BDBV-Nb02	1	2.05E+05	1.77E-04	56.9

Fig. 2. Biophysical characterization of BDBV-Nb01 and BDBV-Nb02. **A, B** Binding kinetics of BDBV-Nb01 (**A**) and BDBV-Nb02 (**B**) to recombinant BDBV GP1, measured by Bio-layer interferometry (BLI). Purified nanobodies were injected at concentrations from 4 to 64 nM; black lines indicate global fitting to a 1:1 binding model. **C, D** Secondary structure analysis by Far-UV CD spectroscopy at 25 °C, showing characteristic β-sheet profiles. **E, F** Thermal stability analysis of BDBV-Nb01 (**E**) and BDBV-Nb02 (**F**). Molar ellipticity was monitored at 218 nm while increasing temperature from 25 °C to 95 °C; melting temperatures (Tm) are indicated. **G** Summary table of kinetic constants (K_{on}, K_{off}, K_D) and thermal stability parameters.

(Fig. 5E). To validate these residues, site-directed mutagenesis was introduced into the BDBV GP protein, and pseudoviruses carrying single or double mutations were tested for neutralization by 2-2-HIS. Our study found that the F248A and the NP278/279AA mutation significantly reduced the neutralizing activity of the 2-2-HIS system against the pseudovirus, whereas L239A and K276A had minimal impact (Fig. 5C–F). These results demonstrate that residues F248, N278, and P279 are the key neutralizing sites for BDBV-Nb02, and confirm the docking.

DISCUSSION

Although licensed antibody therapeutics like Ebanga and Inmazeb significantly improve Ebola disease, their efficacy is primarily limited to EBOV, leaving species like BDBV inadequately covered (Qiu et al., 2014; Howell et al., 2016; Bornholdt et al., 2019; Gilchuk et al., 2020, 2021). The high genetic diversity and rapid evolution of orthoebolaviruses make broad-spectrum neutralizing agents an urgent unmet need.

In this study, we identified BDBV-Nb02, a nanobody with nanomolar affinity and potent neutralizing activity against both EBOV and BDBV pseudoviruses. Compared with previously reported Ebola virus nanobodies that mainly target EBOV, BDBV-Nb02 expands the antiviral spectrum and provides a promising candidate for therapeutic development. Importantly, although direct binding kinetic measurements using purified GP1 mutant proteins would provide further biochemical validation, the significant reduction in neutralizing activity observed in our pseudovirus system due to key mutations provides strong evidence. Our structural and functional analyses revealed that this nanobody recognizes the conserved glycan cap cleft, with residues F248 and NP278/279 being critical for neutralization. This epitope is partially shared with human monoclonal antibodies such as EBOV-437 and EBOV-548, but

A

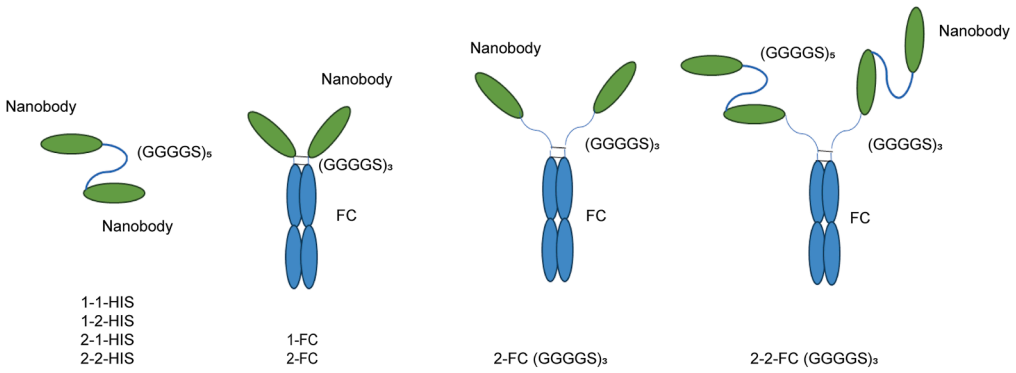

B

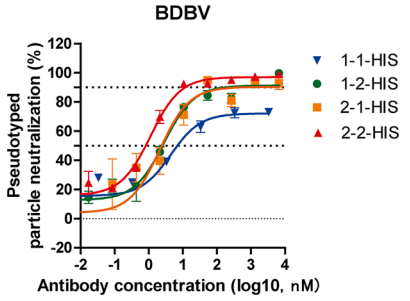

C

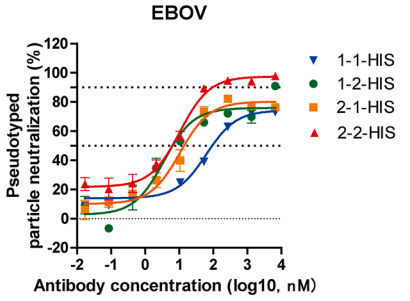

D

		IC50 (nM)	IC90 (nM)	Fold change
BDBV	1-1-HIS	73.68	/	/
	1-2-HIS	3.02	223.8	2.93
	2-1-HIS	3.38	830.5	0.82
	2-2-HIS	1.82	12.18	56.15
EBOV	1-1-HIS	93.54	/	/
	1-2-HIS	6.44	/	/
	2-1-HIS	14.69	/	/
	2-2-HIS	7.23	106.7	3

E

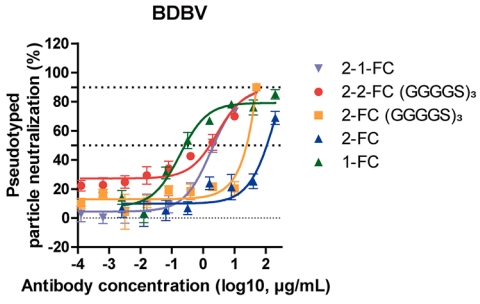

F

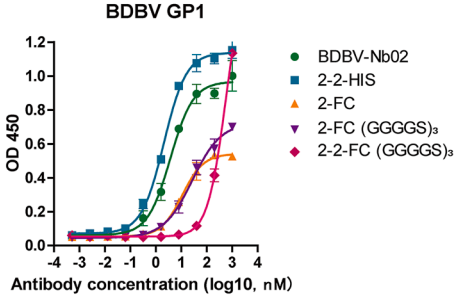

G

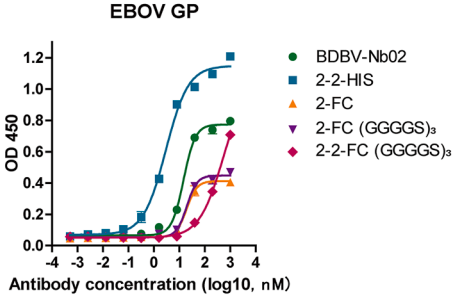

H

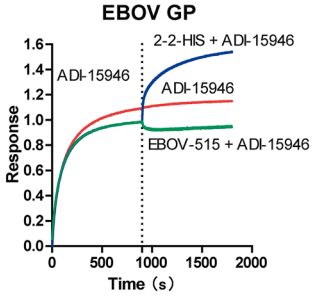

I

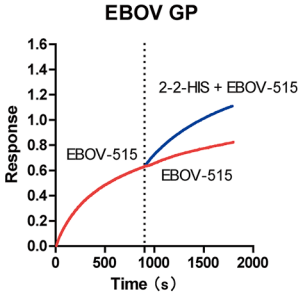

(caption on next page)

Fig. 3. Design and functional evaluation of multivalent BDBV-Nb02 constructs. **A** Schematic illustration of engineered BDBV-Nb02 variants. In the bivalent nanobody and Fc fusion constructs, "1" and "2" represent BDBV-Nb01 and BDBV-Nb02, respectively. **B, C** Neutralization profiles of bivalent constructs against BDBV (**B**) and EBOV (**C**) pseudoviruses. Assays were performed using 5-fold serial dilutions starting from 150 μg/mL. **D** Comparison of half-maximal inhibitory concentration (IC_{50}) and 90% inhibitory concentration (IC_{90}) values between monovalent and bivalent constructs, highlighting the fold-improvement in potency. **E** Neutralization assays of Fc-fused nanobody constructs against BDBV pseudovirus. **F, G** ELISA-based binding assessment of BDBV-Nb02 monomer and engineered bivalent/Fc-fusion variants. Concentration-dependent binding curves of the five indicated antibody constructs against recombinant BDBV GP1 (**F**) and EBOV GP (**G**) protein. Serially diluted antibodies were evaluated by ELISA, with binding responses measured at OD_{450}. The data demonstrate distinct apparent affinities among the engineered architectures. **H, I** Bio-layer interferometry-based epitope competition assay. Biosensors immobilized with full-length GP were saturated with the indicated primary Base-targeting antibodies: ADI-15946 (**H**) or EBOV-515 (**I**). Subsequently, a mixture containing the primary antibody and the competing antibody was introduced (indicated by the dashed line). The robust secondary binding signal confirms that 2-2-HIS does not compete with either ADI-15946 or EBOV-515, demonstrating that its epitope is spatially distinct from the GP Base region.

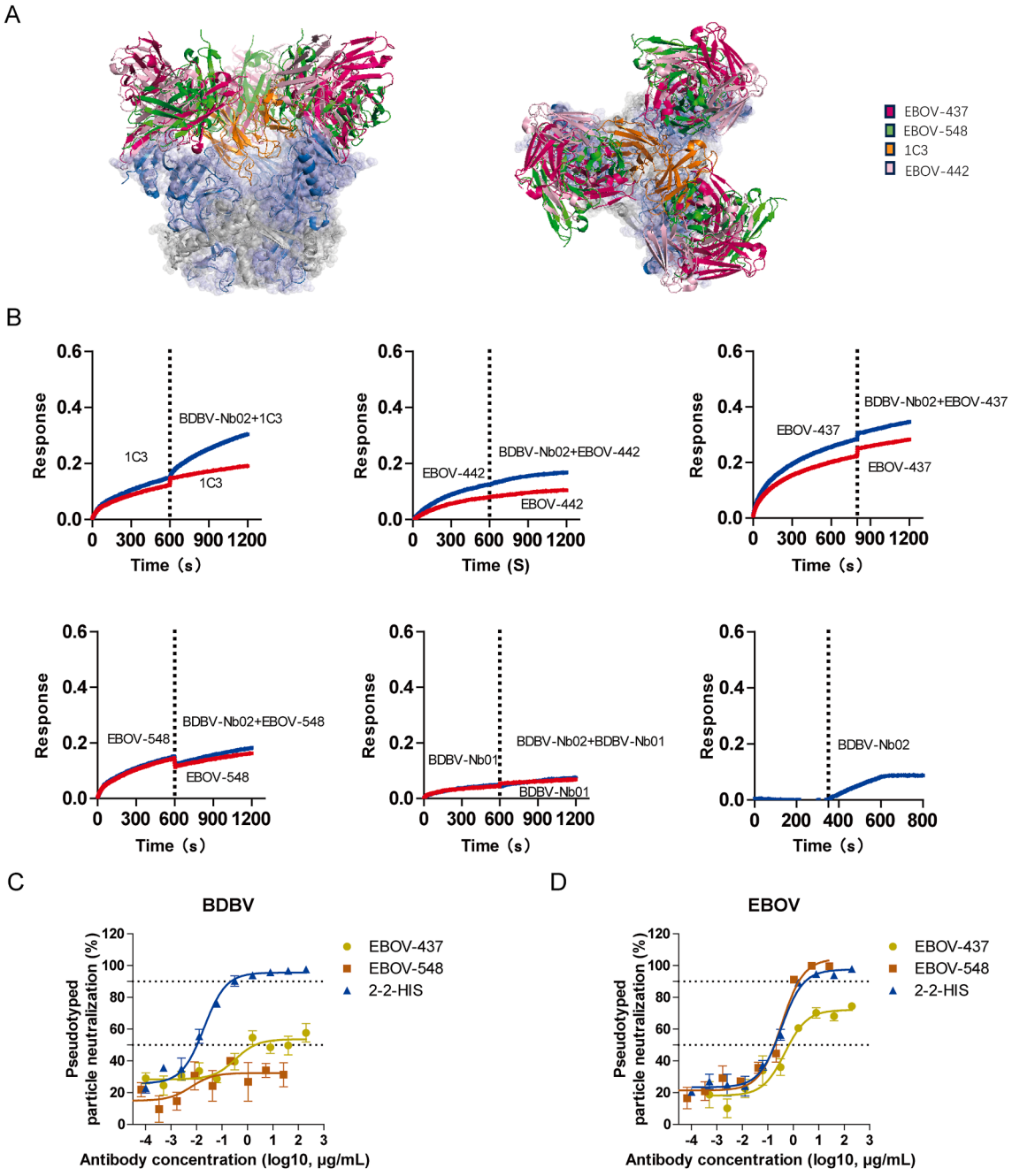

Fig. 4. Epitope mapping of BDBV-Nb02 and functional comparison with epitope-specific antibodies. **A** Schematic representation of neutralizing antibodies targeting the GP1 region. **B** Epitope competition analysis between BDBV-Nb02 and other GP1-targeting antibodies. BDBV GP1 pre-bound biosensors were saturated with a primary antibody followed by BDBV-Nb02. Competitive interference by EBOV-437, 548, 442, and Nb01—but not the RBD-targeting 1C3—localizes the BDBV-Nb02 epitope to the glycan cap. **C** Pseudovirus neutralization assays of 2-2-HIS, EBOV-437, and EBOV-548 against BDBV. **D** Comparative neutralization profiles of 2-2-HIS, EBOV-437, and EBOV-548 against EBOV.

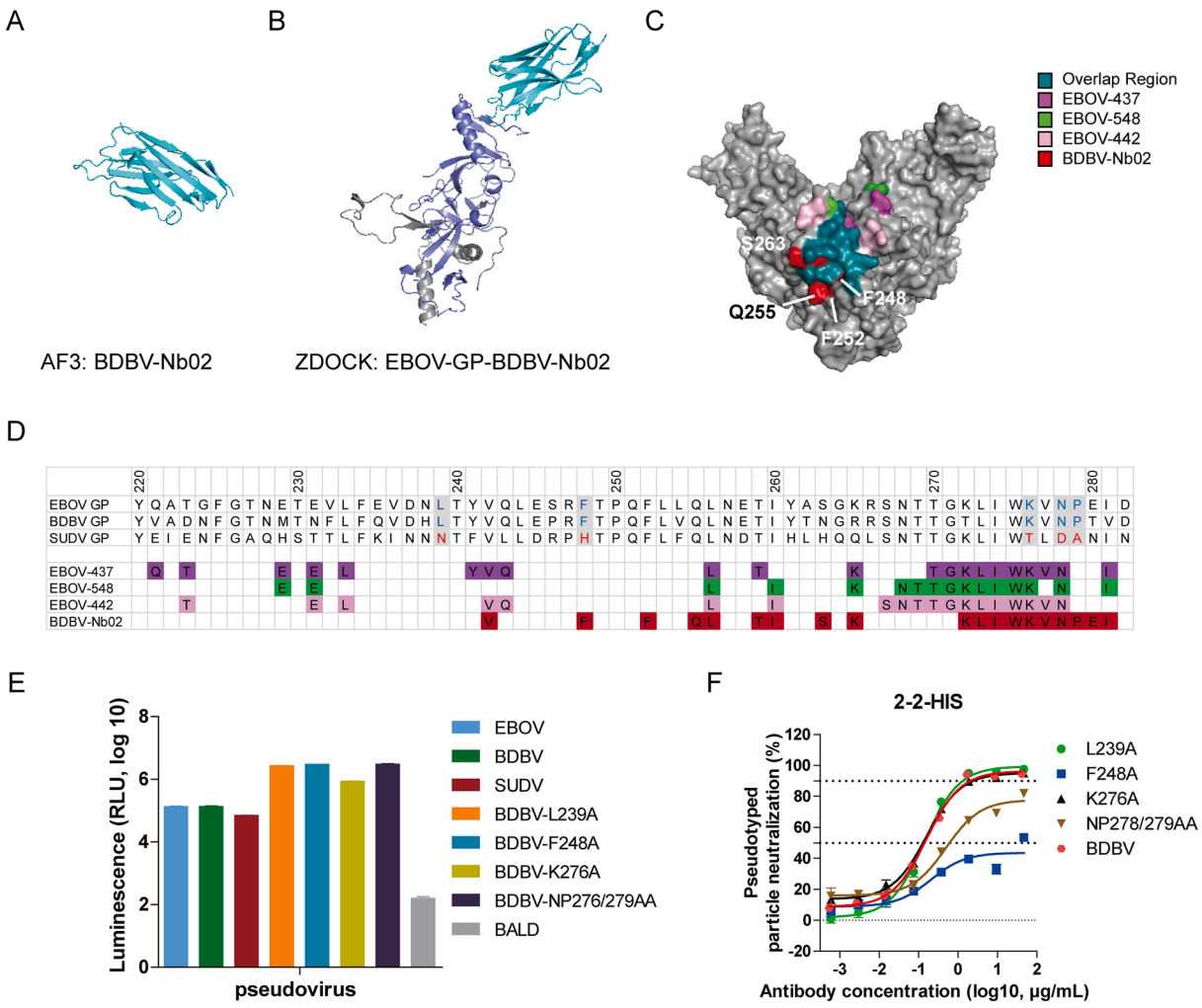

Fig. 5. Identification of critical residues for BDBV-Nb02-mediated neutralization. **A** Structural model of BDBV-Nb02 predicted by AlphaFold 3. **B** Docking model of BDBV-Nb02 in complex with BDBV GP. **C** Location of predicted BDBV-Nb02 binding sites on the GP structure. **D** Sequence alignment of GP residues 220–282 from EBOV, BDBV, and SUDV, highlighting the footprint of BDBV-Nb02 relative to other antibodies. **E** Quality control of pseudovirus stocks, showing luciferase reporter activity (RLU) as a measure of entry infectivity in Huh-7 cells. **F** Effects of GP point mutations on BDBV-Nb02-mediated pseudovirus neutralization. BDBV pseudoviruses harboring alanine substitutions at L239, F248, K276, or N278/P279 were tested against 2-2-HIS. Significant loss of neutralization in F248A and N278A/P279A mutants identifies these as key residues in the functional epitope.

BDBV-Nb02 demonstrated superior activity in the pseudovirus system, highlighting the potential of nanobody scaffolds to exploit unique antigenic sites.

Our engineering studies further demonstrated that a bivalent format (2-2-HIS) markedly enhanced neutralizing potency, achieving up to a 56-fold improvement in IC_{90} compared with the monomeric form. In contrast, fusion with an Fc fragment reduced activity. This contrast suggests that the small size and extended CDR3 loop of nanobodies are essential for accessing glycan-shielded epitopes. Accordingly, an important design principle for nanobody optimization is to preserve these structural features that enable access to sterically restricted regions.

Beyond therapeutic potential, our work also illustrates a methodological advance. By integrating phage display, AlphaFold-based structure prediction, epitope competition assays, and targeted mutagenesis, we established a rapid and cost-effective strategy to define antigen-antibody interactions without relying on high-resolution structural determination. Such an approach could accelerate the discovery of neutralizing antibodies during future outbreaks, when timely intervention is critical.

Nevertheless, this study has several limitations. First, due to the lack of a BSL-4 laboratory, we were not able to demonstrate the neutralizing effect of BDBV-Nb02 on live viruses. Although many studies are currently demonstrating the ability of the Ebola pseudovirus system to detect antibody neutralizing activity (Liu et al., 2023; Fan et al., 2024), *in vivo* validation in animal models is required to confirm protective efficacy. Additionally, while BDBV-Nb02 neutralized both EBOV and BDBV, it showed no activity against SUDV, reflecting the continued challenge of achieving pan-orthoebolavirus coverage. Expanding library screening and rational epitope-guided design may help address this gap.

In summary, BDBV-Nb02 represents a promising broad-spectrum nanobody targeting a conserved glycan cap epitope on orthoebolavirus GP. Its favorable binding properties, resistance to Fc-mediated ADE, and enhanced potency in bivalency form highlight its potential for therapeutic development. More broadly, this study provides a framework for rapid nanobody discovery and optimization, contributing to preparedness against future filovirus outbreaks. Nevertheless, validation using authentic orthoebolaviruses in BSL-4 settings will be required to fully establish therapeutic efficacy in future studies.

CONCLUSIONS

In this study, we identified a broadly active nanobody BDBV-Nb02, which targets a conserved epitope on the GP protein, that effectively

neutralizes both EBOV and BDBV (IC_{50} as low as 1 nM). Engineering a bivalency format markedly enhanced its potency, while Fc fusion impaired activity, underscoring the structural principles critical for nanobody optimization. Epitope mapping and mutagenesis revealed F248 and NP278/279 as key neutralization residues, providing mechanistic insights into glycan-shielded antigen recognition. Together, these findings establish BDBV-Nb02 as a promising candidate for broad orthoebolavirus therapy and highlight the utility of the phage platform for rapidly developing highly effective nanobodies during emerging epidemics.

MATERIALS AND METHODS

Library design and construction

A synthetic phage display library ($> 1.2 \times 10^{10}$ independent clones) was constructed using an optimized, humanized single-domain antibody scaffold. Framework regions (FR) 1, 3, and 4 were humanized to minimize immunogenicity, while camelid-specific residues in FR2 were retained for structural integrity. Complementarity-determining regions (CDRs) were designed based on natural VHH repertoire statistics: CDR1 and CDR2 contained fixed-length diversity (8 aa each), whereas CDR3 varied (16–18 aa) to target cryptic epitopes. Cysteines and stop codons were excluded. Sequencing of $>$ 1000 random clones confirmed $>$ 95% were full-length and unique, demonstrating high diversity and integrity (Chi et al., 2020).

Cells and reagents

The 293T, 293 F, and Huh-7 cell lines were acquired from the China Infrastructure of Cell Line Resource (Beijing, China) and grown in Dulbecco's Modified Eagle's medium (DMEM; Thermo Fisher, Waltham, MA, USA), enriched with 2%–10% fetal bovine serum (FBS; Thermo Fisher, Waltham, MA, USA), non-essential amino acids, penicillin, and streptomycin. Recombinant proteins, including BDBV GP1 (BEP-V5221), were sourced from AcroBiosystems (Beijing, China), and EBOV GP (40442-V08H4-100) were sourced from Sino Biological (Beijing, China).

Antibody selection via phage display

Anti-BDBV GP1 nanobodies were isolated from a proprietary synthetic library through four rounds of panning under standard conditions. For rounds 2 and 4, immunotubes were coated with BDBV GP1 (5 μg/mL). In rounds 1 and 3, biotinylated RBD was captured on streptavidin-coated magnetic beads (Thermo Fisher, Waltham, MA, USA). All surfaces were blocked with 2% skim milk in PBS. Approximately 1×10^{13} phage particles were incubated with antigen for 2 h at 25 °C with gentle shaking. Unbound phage was removed by extensive washing, and bound phage was eluted with 0.1 M glycine-HCl (pH 3.0), neutralized, and used to infect *E. coli* TG1 cells.

After the final round, above 500 individual clones were screened by phage ELISA using BDBV-GP1-coated plates and anti-CM13-HRP. Positive clones were sequenced, and 15 unique nanobody sequences were selected for further expression and analysis.

Expression and purification of nanobodies

Selected nanobody sequences were PCR-amplified (Supplementary Table S1), cloned into the pET-22b vector (Novagen, Sacramento, CA, USA) via *Nco*I/*Xho*I sites, and transformed into *E. coli* BL21 (DE3). A single colony was used to inoculate a starter culture in Luria-Bertani medium with ampicillin (100 μg/mL). This preculture was diluted 1:100 into 400 mL of fresh medium and grown at 37 °C to mid-log phase (OD600 ≈ 0.4–0.6). Protein expression was induced with 0.2 mM Isopropyl β-D-thiogalactoside (IPTG, followed by overnight incubation at 20 °C. The nanobodies, with a His-tag attached at the C-terminus, were purified using Ni Sepharose 6 Fast Flow (GE Healthcare, Boston, MA, USA) and eluted with 400 mM imidazole. Affinity-purified nanobodies were dialyzed against PBS to remove imidazole.

Affinity measurement

SPR experiments were performed on a Biacore T200 instrument (GE Healthcare, Boston, MA, USA) using CM5 sensor chips at 25 °C. The sensor surface was activated with a 1:1 mixture of 0.1 M NHS and 0.1 M EDC at a flow rate of 10 μL/min. A reference flow cell was left unmodified for background subtraction. All surfaces were blocked with 1 M ethanolamine (pH 8.0). Running buffer was PBS supplemented with 0.05% surfactant P20 (PBSP).

For affinity measurements, BDBV GP1 was diluted in 10 mM sodium acetate (pH 5.5) and immobilized to approximately 1000 response units (RU). Serial dilutions of BDBV-Nb01 and BDBV-Nb02 (4–64 nM) were injected over the chip surface. The sensor was regenerated between cycles with 10 mM glycine-HCl (pH 2.5). Data were analyzed using a 1:1 steady-state binding model in BIAevaluation 1.0 software (GE Healthcare, Boston, MA, USA).

Enzyme-linked immunosorbent assay (ELISA)

Antigen-binding capacities were assessed by ELISA. Microtiter plates were coated with recombinant BDBV GP1 or EBOV GP at 2 μg/mL were blocked with 4% non-fat milk in PBS. Nanobody constructs (BDBV-Nb02, 2-2-HIS, 2-Fc, 2-Fc $(GGGGS)_3$, and 2-2-Fc $(GGGGS)_3$) were serially diluted 5-fold in (starting at 1 μM), and incubated for 1 h at 25 °C. Following PBST washes, plates were incubated with HRP-conjugated anti-VHH antibody (A01861, GenScript) for 1 h. Reaction was developed using TMB substrate, stopped with 2 M H_2SO_4, and absorbance was measured at 450 nm. Assays were performed in duplicate, and the data were analyzed using GraphPad Prism (GraphPad Software, California, USA).

Competition-binding assays

Competition-binding experiments were performed using a ForteBio Octet RED96e instrument (BLI). BDBV GP1 (20 μg/mL in 10 mM sodium acetate buffer, pH 5.5) was immobilized on AR2G biosensors (Sartorius, Octet, Göttingen, Germany). All antibodies were diluted to 200 nM in PBS containing 0.02% Tween-20 (PBST).

A two-step assay was designed to assess epitope overlap. First, the antigen-coated sensor was saturated with antibody A. Then, the same sensor was exposed to a mixture containing both antibody A and antibody B. If antibody B failed to bind in the presence of saturated antibody A, this indicated that their epitopes overlap or are spatially adjacent. Conversely, a new binding signal indicated non-overlapping epitopes.

Background binding was corrected using an uncoated reference sensor. After each cycle, the sensor was regenerated with 10 mM glycine-HCl, pH 2.5.

Orthoebolavirus pseudotyped particle (EBOV GP-2pp, BDBV GP-2pp, SUDV GP-2pp)

HEK293T cells were plated in 10-cm dishes at 2.5×10^6 cells/dish one day before transfection. Cells were transfected using Lipofectamine 2000 (Invitrogen, CA, USA) with a mixture containing 10 μg pNL-4.3-Luc-E^-R^- and 10 μg pcDNA-EBOV GP (Ruibiotech) (Millet et al., 2019). A glycoprotein-deficient ('bald') pseudovirus was produced in parallel as a negative control. At 16 h post-transfection, medium was replaced with fresh DMEM containing 2% FBS. Virus-containing supernatants were harvested 36–48 h later, filtered through a 0.22-μm membrane, and used fresh or stored at −80 °C. The BOV-GP protein used for the pcDNA construct corresponds to GenBank accession number AF086833.2 (updated on 2012-2-13). The BDBV-GP protein corresponds

to GenBank accession number MK028856.1 (updated on 2019-7-23), and the SUDV-GP protein corresponds to GenBank accession number YP_138523.1 (updated on 2018-8-13).

The standards for constructing pseudoviruses are as follows, (i) Infectivity: Huh-7 cells were infected with each batch in the absence of inhibitors. Only batches yielding luciferase signals > 100-fold above background (cell-only control) at 48 h post-infection were used in neutralization assays. (ii) Specificity: Parallel infections with pseudoviruses bearing a heterologous glycoprotein (VSV-G) or no glycoprotein ('bald' virus) were performed. Specific entry was confirmed only for EBOV/BDBV/SUDV GP-pseudotyped particles.

Production of human IgG 1 Fc fusion nanobodies or human immunoglobulin G (IgG)

Selected nanobody sequences, along with human IgG heavy and light chains, were cloned into a mammalian expression vector under control of the hEF1-HTLV promoter. The vector included an N-terminal interleukin-2 signal peptide and a C-terminal Fc region comprising the hinge, CH2, and CH3 domains of human IgG1. Plasmids were prepared by maxiprep and transiently transfected into suspension-adapted 293F cells. After five days of culture, supernatants were harvested, and Fc-fusion proteins were purified using Protein A affinity chromatography (GenScript, China). Protein integrity, dimerization, yield, and purity were assessed by SDS-PAGE and Western blot under standard conditions.

BDBV GP plasmid point mutation

Following the sequence alignment analysis results, BDBV GP mutation sites were identified using the Mut Express II Fast Mutagenesis Kit (Vazyme, China). Forward and reverse primers, ranging from 18 to 25 base pairs in length with melting temperatures (Tm) of at least 60 °C, were designed to target the mutation sites. PCR amplification was performed with high-fidelity DNA polymerase, using the BDBV GP plasmid as the template. Then transformed into competent cells. Positive clones were selected and sequenced to verify the mutation sites, with successful mutants used in subsequent experiments.

Neutralization assay

To perform the virus entry assay, Huh-7 cells were seeded into each well of a 96-well plate one day before transduction. The following day, 100 μL of supernatant containing orthoebolavirus GP pseudotyped particles was added to each well, with or without serially diluted monoclonal antibodies (mAb). Forty-eight hours after transduction, the cells were lysed in 100 μL of passive lysis buffer, and 50 μL of the lysate was combined with 100 μL of luciferase assay substrate, following the manufacturer's instructions (Promega, Madison, WI, USA).

AlphaFold 3 prediction

For AlphaFold 3 (AF3) predictions, the ADI-15946-EBOV GP complex (PDB: 6MAM) was modeled using GP sequences (copies = 3) alongside the antibody heavy and light chains (copies = 1). Subsequent BDBV-Nb02 structural predictions were performed using the nanobody primary sequence (copies = 1) (Abramson et al., 2024).

Molecular docking

To model the BDBV-Nb02-GP interaction, we combined computational and experimental approaches. The BDBV-Nb02 structure was predicted using AlphaFold3. Molecular docking was then performed with spatial constraints derived from (Pierce et al., 2014) (i) competitive binding assays, which localized the epitope to the GP1 region (residues Y220-D282) shared with antibodies EBOV-437, EBOV-548, and BDBV-442, and (ii) sequence alignment, which identified EBOV/BDBV-conserved but SUDV-divergent residues (L239, F248, K276, NP278/279) as putative contact sites. Ten representative docking models were generated under these constraints. These models served as working hypotheses, with final epitope mapping dependent on experimental validation via site-directed mutagenesis.

Statistics and reproducibility

Data were analyzed using GraphPad Prism 5 (GraphPad Software, California, USA) and are presented as mean ± SD. For neutralization assays, infectivity values were converted to percent neutralization, normalized to virus-only controls (0%) and cell-only backgrounds (100%). Dose-response curves were fitted using a four-parameter nonlinear regression model to calculate half-maximal inhibitory concentrations (IC_{50}). Experiments included four replicate wells per condition and were performed independently at least twice with consistent results; figures show representative data from one experiment.

DATA AVAILABILITY

All the data generated during the current study are included in the manuscript. This paper does not report original code. Any additional information required to reanalyze the data reported in this paper is available from the lead contact upon request. Lead contact: chixiaojing@ipbcams.ac.cn, wyang@ipb.pumc.edu.cn.

ETHICS STATEMENT

This article does not contain any studies with human or animal subjects performed by any of the authors.

AUTHOR CONTRIBUTIONS

Xinhui Zhang: conceptualization data curation, formal analysis, investigation; methodology, resources, software, validation, visualization, writing-original draft. Yi Liao: investigation. Xiuying Liu: project administration. Jingya Zhou: investigation, Peixiang Gao: investigation. Xuemeng Dong: investigation. Shengnan Pan: investigation. Huarui Duan: investigation. Junyu Liu: investigation. Xiaojing Chi: writing-review & editing, conceptualization, funding acquisition. Wei Yang: conceptualization, funding acquisition, writing-review & editing.

CONFLICT OF INTEREST

A patent application has been filed for BDBV-Nb02 (Application No. 202510326241.3).

ACKNOWLEDGMENTS

This study was supported by grants from the National Natural Science Foundation of China (U22A20553 and 82241064), the Chinese Academy of Medical Sciences Innovation Fund for Medical Sciences (2025-I2M-KJ-022 and 2021-I2M-1-038), and the Fundamental Research Funds for the Central Universities of Peking Union Medical College (3332024204). We thank the Core Facilities and Service Centers of National Institute of Pathogen Biology, CAMS and PUMC for assistance with instrumentation.

APPENDIX A. SUPPLEMENTARY DATA

Supplementary data to this article can be found online at https://doi.org/10.1016/j.virs.2026.03.018.

REFERENCES

Abramson, J., Adler, J., Dunger, J., Evans, R., Green, T., Pritzel, A., Ronneberger, O., Willmore, L., Ballard, A.J., Bambrick, J., Bodenstein, S.W., Evans, D.A., Hung, C.C., O'Neill, M., Reiman, D., Tunyasuvunakool, K., Wu, Z., Zemgulyte, A., Arvaniti, E., Beattie, C., Bertolli, O., Bridgland, A., Cherepanov, A., Congreve, M., Cowen-Rivers, A.I., Cowie, A., Figurnov, M., Fuchs, F.B., Gladman, H., Jain, R., Khan, Y.A., Low, C.M.R., Perlin, K., Potapenko, A., Savy, P., Singh, S., Stecula, A., Thillaisundaram, A., Tong, C., Yakneen, S., Zhong, E.D., Zielinski, M., Zidek, A., Bapst, V., Kohli, P., Jaderberg, M., Hassabis, D., Jumper, J.M., 2024. Addendum: accurate structure prediction of biomolecular interactions with AlphaFold 3. Nature 636, E4.

Bornholdt, Z.A., Herbert, A.S., Mire, C.E., He, S.H., Cross, R.W., Wec, A.Z., Abelson, D. M., Geisbert, J.B., James, R.M., Rahim, N., Zhu, W.J., Borisevich, V., Banadyga, L., Gunn, B.M., Agans, K.N., Wirchnianski, A.S., Goodwin, E., Tierney, K., Shestowsky, W.S., Bohorov, O., Bohorova, N., Velasco, J., Ailor, E., Kim, D., Pauly, M.H., Whaley, K.J., Alter, G., Walker, L.M., Chandran, K., Zeitlin, L., Qiu, X. G., Geisbert, T.W., Dye, J.M., 2019. A two-antibody Pan-Ebolavirus cocktail confers broad therapeutic protection in ferrets and nonhuman Primates. Cell Host Microbe 25, 49–58.e5.

Caballero, I.S., Honko, A.N., Gire, S.K., Winnicki, S.M., Melé, M., Gerhardinger, C., Lin, A.E., Rinn, J.L., Sabeti, P.C., Hensley, L.E., Connor, J.H., 2016. In vivo Ebola virus infection leads to a strong innate response in circulating immune cells. BMC Genom. 17, 707.

Chi, X.J., Liu, X.Y., Wang, C.H., Zhang, X.H., Li, X., Hou, J.H., Ren, L.L., Jin, Q., Wang, J. W., Yang, W., 2020. Humanized single domain antibodies neutralize SARS-CoV-2 by targeting the spike receptor binding domain. Nat. Commun. 11, 4528.

Chi, X.J., Zhang, X.H., Pan, S.N., Yu, Y.Y., Shi, Y.J., Lin, T.L., Duan, H.R., Liu, X.Y., Chen, W.F., Yang, X.H., Chen, L., Dong, X.Q., Ren, L.L., Ding, Q., Wang, J.W., Yang, W., 2022. An ultrapotent RBD-targeted biparatopic nanobody neutralizes broad SARS-CoV-2 variants. Signal Transduct. Targeted Ther. 7, 44.

Corti, D., Misasi, J., Mulangu, S., Stanley, D.A., Kanekiyo, M., Wollen, S., Ploquin, A., Doria-Rose, N.A., Staupe, R.P., Bailey, M., Shi, W., Choe, M., Marcus, H., Thompson, E.A., Cagigi, A., Silacci, C., Fernandez-Rodriguez, B., Perez, L., Sallusto, F., Vanzetta, F., Agatic, G., Cameroni, E., Kisalu, N., Gordon, I., Ledgerwood, J.E., Mascola, J.R., Graham, B.S., Muyembe-Tamfun, J.J., Trefry, J.C., Lanzavecchia, A., Sullivan, N.J., 2016. Protective monotherapy against lethal Ebola virus infection by a potently neutralizing antibody. Science 351, 1339–1342.

Divine, R., Dang, H., Ueda, G., Fallas, J.A., Vulovic, I., Sheffler, W., Saini, S., Zhao, Y.T., Raj, I.X., Morawski, P.A., Jennewein, M.F., Homad, L.J., Wan, Y.H., Tooley, M.R., Seeger, F., Etemadi, A., Fahning, M.L., Lazarovits, J., Roederer, A., Walls, A.C., Stewart, L., Mazloomi, M., King, N.P., Campbell, D.J., McGuire, A.T., Stamatatos, L., Ruohola-Baker, H., Mathieu, J., Veesler, D., Baker, D., 2021. Designed proteins assemble antibodies into modular nanocages. Science 372, eabd9994.

Escudero-Pérez, B., Volchkova, V.A., Dolnik, O., Lawrence, P., Volchkov, V.E., 2014. Shed GP of Ebola virus triggers immune activation and increased vascular permeability. PLoS Pathog. 10, e1004509.

Fan, P.F., Sun, B.J., Liu, Z.X., Fang, T., Ren, Y., Zhao, X.F., Song, Z.W., Yang, Y.L., Li, J.M., Yu, C.M., Chen, W., 2024. A pan-orthoebolavirus neutralizing antibody encoded by mRNA effectively prevents virus infection. Emerg. Microb. Infect. 13, 2432366.

Feldmann, H., Geisbert, T.W., 2011. Ebola haemorrhagic fever. Lancet 377, 849–862.

Gilchuk, P., Murin, C.D., Cross, R.W., Ilinykh, P.A., Huang, K., Kuzmina, N., Borisevich, V., Agans, K.N., Geisbert, J.B., Zost, S.J., Nargi, R.S., Sutton, R.E., Suryadevara, N., Bombardi, R.G., Carnahan, R.H., Bukreyev, A., Geisbert, T.W., Ward, A.B., Crowe, J., 2021. Pan-ebolavirus protective therapy by two multifunctional human antibodies. Cell 184, 5593–5607.e18.

Gilchuk, P., Murin, C.D., Milligan, J.C., Cross, R.W., Mire, C.E., Ilinykh, P.A., Huang, K., Kuzmina, N., Altman, P.X., Hui, S., Gunn, B.M., Bryan, A.L., Davidson, E., Doranz, B. J., Turner, H.L., Alkutkar, T., Flinko, R., Orlandi, C., Carnahan, R., Nargi, R., Bombardi, R.G., Vodzak, M.E., Li, S., Okoli, A., Ibeawuchi, M., Ohiaeri, B., Lewis, G. K., Alter, G., Bukreyev, A., Saphire, E.O., Geisbert, T.W., Ward, A.B., Crowe, J.E., 2020. Analysis of a therapeutic antibody cocktail reveals determinants for cooperative and broad Ebolavirus neutralization. Immunity 52, 388–403.e12.

Han, Q., Wang, S., Wang, Z., Zhang, C., Wang, X., Feng, N., Wang, T., Zhao, Y., Chi, H., Yan, F., Xia, X., 2023. Nanobodies with cross-neutralizing activity provide prominent therapeutic efficacy in mild and severe COVID-19 rodent models. Virol. Sin. 38, 787–800.

Howell, K.A., Qiu, X.G., Brannan, J.M., Bryan, C., Davidson, E., Holtsberg, F.W., Wec, A. Z., Shulenin, S., Biggins, J.E., Douglas, R., Enterlein, S.G., Turner, H.L., Pallesen, J., Murin, C.D., He, S.H., Kroeker, A., Vu, H., Herbert, A.S., Fusco, M.L., Nyakatura, E. K., Lai, J.R., Keck, Z.Y., Foung, S.K.H., Saphire, E.O., Zeitlin, L., Ward, A.B., Chandran, K., Doranz, B.J., Kobinger, G.P., Dye, J.M., Aman, M.J., 2016. Antibody treatment of Ebola and Sudan virus infection via a uniquely exposed epitope within the Glycoprotein receptor-binding site. Cell Rep. 15, 1514–1526.

Hutchinson, K.L., Rollin, P.E., 2007. Cytokine and chemokine expression in humans infected with Sudan Ebola virus. JID (J. Infect. Dis.) 196 (Suppl. 2), S357–S363.

Lee, J.E., Fusco, M.L., Hessell, A.J., Oswald, W.B., Burton, D.R., Saphire, E.O., 2008. Structure of the ebola virus glycoprotein bound to an antibody from a human survivor. Nature 454, 177–182.

Liu, G.D., He, S.H., Chan, M.C., Zhang, Z.R., Schulz, H., Cao, W.G., Rahim, M.N., Audet, J., Garnett, L., Wec, A., Chandran, K., Qiu, X.G., Banadyga, L., 2023. A pan-ebolavirus monoclonal antibody cocktail provides protection against ebola and Sudan viruses. JID (J. Infect. Dis.) 228 (Suppl. 7), S691–S700.

Millet, JK, Tang, T, Nathan, L, et al., 2019. Production of pseudotyped particles to study highly pathogenic coronaviruses in a biosafety level 2 setting. J Vis Exp (145). https://doi.org/10.3791/59010. Published 2019 Mar 1.

Mulangu, S., Dodd, L.E., Davey, R.T., Mbaya, O.T., Proschan, M., Mukadi, D., Manzo, M. L., Nzolo, D., Oloma, A.T., Ibanda, A., Ali, R., Coulibaly, S., Levine, A.C., Grais, R., Diaz, J., Lane, H.C., Muyembe-Tamfum, J.J., Sivahera, B., Camara, M., Kojan, R., Walker, R., Dighero-Kemp, B., Cao, H.Y., Mukumbayi, P., Mbala-Kingebeni, P., Ahuka, S., Albert, S., Bonnett, T., Crozier, I., Duvenhage, M., Proffitt, C., Teitelbaum, M., Moench, T., Aboulhab, J., Barrett, K., Cahill, K., Cone, K., Eckes, R., Hensley, L., Herpin, B., Higgs, E., Ledgerwood, J., Pierson, J., Smolskis, M., Sow, Y., Tierney, J., Sivapalasingam, S., Holman, W., Gettinger, N., Vallée, D., Nordwall, J., Grp, P.W., Team, P.C.S., 2019. A randomized, controlled trial of ebola virus disease therapeutics. N. Engl. J. Med. 381, 2293–2303.

Pallesen, J., Murin, C.D., de Val, N., Cottrell, C.A., Hastie, K.M., Turner, H.L., Fusco, M.L., Flyak, A.I., Zeitlin, L., Crowe, J.E., Andersen, K.G., Saphire, E.O., Ward, A.B., 2016. Structures of ebola virus GP and sGP in complex with therapeutic antibodies. Nat. Microbiol. 1, 16128.

Pierce, B.G., Wiehe, K., Hwang, H., Kim, B.H., Vreven, T., Weng, Z.P., 2014. ZDOCK server: interactive docking prediction of protein-protein complexes and symmetric multimers. Bioinformatics 30, 1771–1773.

Qiu, X.G., Wong, G., Audet, J., Bello, A., Fernando, L., Alimonti, J.B., Fausther-Bovendo, H., Wei, H.Y., Aviles, J., Hiatt, E., Johnson, A., Morton, J., Swope, K., Bohorov, O., Bohorova, N., Goodman, C., Kim, D., Pauly, M.H., Velasco, J., Pettitt, J., Olinger, G.G., Whaley, K., Xu, B.L., Strong, J.E., Zeitlin, L., Kobinger, G.P., 2014. Reversion of advanced ebola virus disease in nonhuman Primates with ZMapp. Nature 514, 47–53.

Rijal, P., Donnellan, F.R., 2023. A review of broadly protective monoclonal antibodies to treat Ebola virus disease. Curr. Opin. Virol. 61, 101339.

Rivera, A., Messaoudi, I., 2016. Molecular mechanisms of Ebola pathogenesis. J. Leukoc. Biol. 100, 889–904.

Schieffelin, J.S., Shaffer, J.G., Goba, A., Gbakie, M., Gire, S.K., Colubri, A., Sealfon, R.S. G., Kanneh, L., Moigboi, A., Momoh, M., Fullah, M., Moses, L.M., Brown, B.L., Andersen, K.G., Winnicki, S., Schaffner, S.F., Park, D.J., Yozwiak, N.L., Jiang, P.P., Kargbo, D., Jalloh, S., Fonnie, M., Sinnah, V., French, I., Kovoma, A., Kamara, F.K., Tucker, V., Konuwa, E., Sellu, J., Mustapha, I., Foday, M., Yillah, M., Kanneh, F., Saffa, S., Massally, J.L.B., Boisen, M.L., Branco, L.M., Vandi, M.A., Grant, D.S., Happi, C., Gevao, S.M., Fletcher, T.E., Fowler, R.A., Bausch, D.G., Sabeti, P.C., Khan, S.H., Garry, R.F., Consortium, V.H.F., Team, W.C.R., 2014. Clinical illness and outcomes in patients with Ebola in Sierra Leone. N. Engl. J. Med. 371, 2092–2100.

Scully, M., Cataland, S.R., Peyvandi, F., Coppo, P., Knöbl, P., Hovinga, J.A.K., Metjian, A., de la Rubia, J., Pavenski, K., Callewaert, F., Biswas, D., De Winter, H., Zeldin, R.K., Investigators, H., 2019. Caplacizumab treatment for acquired thrombotic thrombocytopenic purpura. N. Engl. J. Med. 380, 335–346.

Steeland, S., Vandenbroucke, R.E., Libert, C., 2016. Nanobodies as therapeutics: big opportunities for small antibodies. Drug Discov. Today 21, 1076–1113.

Thomas, S., Smatti, M.K., Ouhtit, A., Cyprian, F.S., Almaslamani, M.A., Al Thani, A., Yassine, H.M., 2022. Antibody-Dependent Enhancement (ADE) and the role of complement system in disease pathogenesis. Mol. Immunol. 152, 172–182.

Wauquier, N., Becquart, P., Padilla, C., Baize, S., Leroy, E.M., 2010. Human fatal Zaire Ebola virus infection is associated with an aberrant innate immunity and with massive lymphocyte apoptosis. PLoS Neglected Trop. Dis. 4, e837.

Younan, P., Iampietro, M., Bukreyev, A., 2018. Disabling of lymphocyte immune response by Ebola virus. PLoS Pathog. 14, e1006932.

Younan, P., Iampietro, M., Nishida, A., Ramanathan, P., Santos, R.I., Dutta, M., Lubaki, N.M., Koup, R.A., Katze, M.G., Bukreyev, A., 2017. Ebola virus binding to Tim-1 on T lymphocytes induces a cytokine storm. mBio 8, e00845-17.

Yu, T., Zheng, F., He, W.B., Muyldermans, S., Wen, Y.R., 2024. Single domain antibody: development and application in biotechnology and biopharma. Immunol. Rev. 328, 98–112.